Theor. Appl. Climatol. 80, 245–257 (2005)
DOI 10.1007/s00704-004-0103-2

Theoretical and Applied Climatology
Printed in Austria

Institute for Atmospheric and Climate Science, ETH Zürich, Switzerland

Prognostic canopy air space solutions for land surface exchanges

P. L. Vidale and **R. Stöckli**

With 5 Figures

Received October 27, 2003; accepted June 23, 2004
Published online December 15, 2004

Summary

Three generations of land surface models have been developed over the course of the last twenty years, which include increasing levels of complexity. The latest generation incorporates photosynthesis and physiological responses to environmental CO_2, a gas that is strongly controlled by atmospheric vertical stability and by land surface exchanges. A new set of prognostic equations, providing a new solution core for one such land surface model, SiB2, is introduced here. The new equation set makes use of canopy air space variables which are prognostic and allow for the storage of heat, water and carbon at that level, providing both a new memory for the coupled system and a better representation of observed canopy processes. Results from off-line simulation using FLUXNET data from Europe, over a range of environmental and climatic conditions, indicate that the new solution core is able to represent land surface exchanges with equal or better skill than the set it replaces. At the same time, this new formulation provides a simplified mathematical framework, more suitable for further model development.

1. Introduction

Soil-vegetation–atmosphere transfer schemes have been used for years in atmospheric models in order to describe the surface exchanges of heat, water, momentum and carbon. Several different strategies are followed in what concerns the complexity of the included bio-physical processes and the horizontal and vertical distribution of flux sources and pathways, which often depend on scaling criteria and target application. Extensive reviews are provided in Arora (2002), Pielke (2001) and in Sellers et al. (1997).

The typical framework of a Land Surface Model (LSM), shown in Fig. 1a, involves the ground surface, snow, canopy leaves and reference level atmosphere as prognostic variables. The model framework comprises individual grid boxes, covered by portions of bare ground, vegetation (as a one-layer elevated canopy) and snow, all interacting with the overlying atmosphere through the canopy air space (CAS), which acts as a flux mediator.

The CAS variables are usually solved for as a weighted average of the ground surface, canopy and reference level variables (see for instance Dickinson et al., 1993 and Bonan, 1996). This layer is, therefore, traditionally described in terms of a combination of the individual leaf, soil, snow and reference level variables, so that it has no properties of its own, and fluxes through it are instantaneously adjusted, with no possibility for time delays in the exchanges. This approach was justified in applications in which the thickness of the first atmospheric level (or the height of the probe) was much larger than the typical thickness of the CAS (order of 10 m). In more modern models, with increased resolution

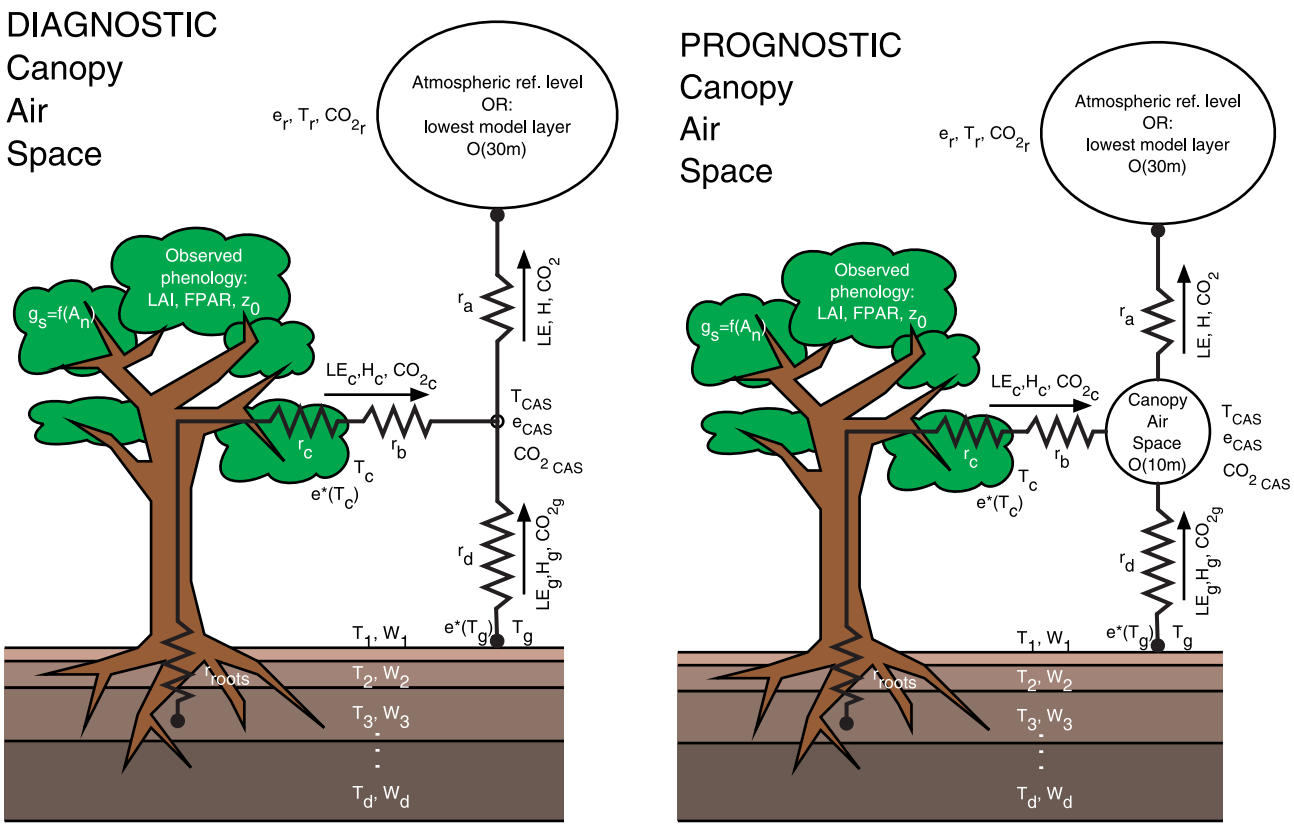

Fig. 1. **a**) The SiB2 land surface model framework: the diagnostic CAS scheme (left) and **b**) the new prognostic CAS (right)

in the boundary layer (BL) and an explicitly resolved surface layer (SL), with a typical height of 30 m, this approach is not completely justified. This can be seen in Table 1, which shows how the typical heat capacities of each variable in the framework have comparable magnitudes, indicating similar potentials for the storage of heat, water vapor and CO_2.

Table 1. Typical heat capacities near the land surface[a]

Variable (level)	Volume (m^3/m^2)	Total heat capacity $MJ/m^2 K$
Air, atmospheric reference[b]	30	0.03
Air, CAS[c]	10	0.01
Canopy leaves[d]	0.003	0.002
Interception water	0.001	0.004
Snow	0.01	0.07
Soil (top)	0.02	0.04

[a] Values extracted from Sellers et al. (1996b)
[b] First atmospheric model level
[c] Canopy Air Space
[d] With LAI = 3

In the practice of flux calculations from eddy correlation tower data it is also recognized that the layer of air below the tower can store individual properties and these storage fluxes are calculated from the vertical divergence of the properties above and below the CAS. From the point of view of observational evidence, the need to consider CAS storage is supported by measurements at several micrometeorological towers (see for instance Schmid et al., 2003 or the FLUXNET data itself, Baldocchi et al., 2001).

Given the observational evidence and new modeling requirements, it would seem necessary to treat the CAS air as a finite vertical layer and not an infinitesimally thin one. We propose to introduce a CAS layer in a LSM framework in order to test the feasibility of such an approach and its degree of physicality.

The SiB2 LSM (Sellers et al., 1996b) has been extensively used in off-line and on-line mode over a wide range of spatial and temporal ranges, examples of which are given in Kim et al. (2001), Randall et al. (1996), Denning et al. (2003). It represents therefore an ideal test bed for this type

of new prognostic approach. The implementation presented here introduces new prognostic variables in correspondence to CAS storage capacities and associated fluxes, similar to what was done by Walko et al. (2000), which require the solution of three new prognostic equations.

The goal of this work is to document the new solution core that was implemented in the model (referred to as SiB2.5) and successfully used by Baker et al. (2003), Denning et al. (2003), and Stöckli and Vidale (2004b) (this issue). The existing solution set is thus initially discussed and the new prognostic core is introduced thereafter, together with some examples of off-line applications. Discretized versions of the prognostic equations, useful for numerical implementation, are presented in the appendix.

2. Prognostic equations at the land surface in SiB2

The governing prognostic equations for the land surface variables, i.e. the heat and water of the ground-snow surface (suffix g) and canopy leaves (suffix c), were introduced in Sellers et al. (1996b) and the temperature relationships are summarized here for reference:

$$c_g \frac{\partial T_g}{\partial t} = R_{n_g} - H_g - E_g - G$$
$$c_c \frac{\partial T_c}{\partial t} = R_{n_c} - H_c - E_c \qquad (1)$$

where $T_{c,g}$ are the temperatures of the canopy leaves and snow-ground (K); $c_{g,c}$ are the effective heat capacities ($\mathrm{J\,m^{-2}\,K^{-1}}$); R, H, E and G are the net radiation, sensible heat flux, latent heat flux and ground heat flux ($\mathrm{W\,m^{-2}}$).

In the SiB2 modeling system the canopy air space acts as an instantaneous mediator between individual flux network components, and all fluxes through the CAS are additive, equaling the fluxes between CAS and the atmospheric reference level, as is explained in the next subsection.

2.1 Canopy air space variables and their diagnostic treatment

Referring again to Fig. 1a (left panel), the canopy air space is the portion of the surface layer which is in direct contact with the canopy leaves and which mediates the turbulent exchanges between leaves, bare ground, snow and the atmospheric reference level above. In reference to the framework of the SiB2 model, in which the present solutions have been implemented, it is the distance between heights z_2 and z_1 (canopy top and canopy base) in Fig. 1 of Sellers et al. (1996b).

In this context, the CAS has a storage capacity equivalent to the volume per square meter in the layer that comprises the vegetation canopy. In the original model of Sellers et al. (1996b), this quantity was considered infinitesimally small, so that the definition for CAS variables in SiB 2.0 are:

$$T_a = \frac{\frac{T_r}{r_a} + \frac{T_c}{r_b} + \frac{T_g}{r_d}}{\frac{1}{r_a} + \frac{1}{r_b} + \frac{1}{r_d}};$$
$$e_a = \frac{\frac{e_r}{r_a} + \frac{e_c}{r_c+2r_b} + \frac{e_g}{r_d}}{\frac{1}{r_a} + \frac{1}{r_c+2r_b} + \frac{1}{r_d}};$$
$$\mathrm{CO_2}_a = \frac{\frac{\mathrm{CO_2}_r}{r_a} + \frac{\mathrm{CO_2}_c}{1.6r_c+2.8r_b} + \frac{\mathrm{CO_2}_g}{r_d}}{\frac{1}{r_a} + \frac{1}{1.6r_c+2.8r_b} + \frac{1}{r_d}} \qquad (2)$$

where $T_{c,g,a,r}$ are the temperatures of the canopy leaves, snow-ground, CAS and reference level (K); $e_{c,g,a,r}$ are the vapor pressures (Pa); $\mathrm{CO_2}_{c,g,a,r}$ are the CO_2 partial pressures (Pa); r_a, r_b, r_c, r_d are the resistances ($\mathrm{s\,m^{-1}}$).

Scalar fluxes through the CAS are correspondingly additive and instantaneously adjusted, equaling therefore fluxes between the CAS and the atmospheric reference level:

$$H_a = H_c + H_g;$$
$$E_a = E_c + E_g = E_{ci} + E_{ct} + E_{gi} + E_{gs};$$
$$F_{\mathrm{CO_2}_a} = F_{\mathrm{CO_2}_c} + F_{\mathrm{CO_2}_g} \qquad (3)$$

where $H_{c,g,a}$ are the sensible heat fluxes from canopy leaves, snow-ground and CAS ($\mathrm{W\,m^{-2}}$); $E_{c,g,a}$ are the latent heat fluxes from canopy leaves, snow-ground and CAS ($\mathrm{W\,m^{-2}}$); $F_{\mathrm{CO_2}_{c,g,a}}$ are the carbon fluxes from canopy leaves, snow-ground and CAS ($\mu\mathrm{mol\,m^{-2}\,s^{-1}}$). The subscripts i, t, s refer to water vapor originating from interception, transpiration and top soil pore reservoirs, respectively.

A limitation of the standard implementation, using the classic weighted average approach to the calculation of the CAS capacity, is that it introduces dependencies on all prognostic

variables when partial derivative terms are calculated, making the calculations cumbersome and preventing the use of the variables in some of the equations (most notably in the calculations of the r_b and r_d aerodynamic exchange coefficients, see Sellers et al., 1996b; Eqs. 10 and 11).

For example, in the case of the canopy leaves heat flux, H_c, Sato et al. (1989a), Sato et al. (1989b) and Sellers et al. (1996b) use a definition of the CAS temperature similar to that in other LSM (e.g. BATS), as was shown in Eq. (2). Because of this definition, the numerous flux cross-derivative terms used in the solution implementation (see the Appendix), for an arbitrary variable S_x, $\frac{\partial F_x}{\partial S_x}$ will contain terms involving all three boundary temperatures, that is the ground, leaves and reference air temperatures.

An example of the extensive and inconvenient flux derivative formulation resulting from this approach in the case of terms involving the heat flux from the canopy leaves, H_c:

$$H_c = \rho c_p \frac{(T_c - T_a)}{r_b}$$

where ρ is the density ($\mathrm{kg\,m^{-3}}$) and c_p is the heat capacity ($\mathrm{J\,kg^{-1}\,K^{-1}}$) of air, so that:

$$\frac{\partial H_c}{\partial T_c} = \rho \frac{c_p}{r_b}\left(1 - \left[\frac{\frac{1}{r_b}}{\frac{1}{r_a}+\frac{1}{r_b}+\frac{1}{r_d}}\right]\right) \tag{4}$$

because of the definitions in Eq. (2).

This approach was fully justified in applications for which the height of the reference level was much larger than the vertical extent of the canopy air space or in coupled systems in which only a bulk mixed layer (and no surface layer) are simulated (such as in the CSU GCM). If the vertical extent of the CAS and the distance to the reference level are of the same order of magnitude, however, a different treatment should be considered, since the capacities of the canopy air space and of the first atmospheric level in the host model are of similar magnitude.

2.2 Canopy air space variables and their prognostic treatment: the new solution core

More modern applications, off-line or coupled, assume that the atmospheric reference level is located much nearer to the surface, so that the heat (water, or any scalar) capacity of the layer of air that it represents is of the same order of magnitude as that of the canopy air space (CAS), that is, the amount of air contained within the (interacting directly with) canopy leaves. It is assumed here that the CAS spans the region between canopy base and top; an idealized picture of this new framework is shown in Fig. 1b.

With both physical and numerical reasons in mind, CAS capacities and variables are proposed, together with corresponding prognostic equations at that vertical level, as was also done previously in Walko et al. (2000), for a simpler LSM. Three new prognostic equations for CAS temperature, water and CO_2 are thus added to the set in Eq. (1):

$$\begin{aligned} c_a \frac{\partial T_a}{\partial t} &= -H_a + H_c + H_g \\ c_a \frac{\partial e_a}{\partial t} &= -E_a + E_c + E_g \\ c_a \frac{\partial \mathrm{CO}_{2_a}}{\partial t} &= -F_{\mathrm{CO}_{2_a}} + F_{\mathrm{CO}_{2_c}} + F_{\mathrm{CO}_{2_g}} \end{aligned} \tag{5}$$

where c_a is the storage capacity of the CAS in $\mathrm{J\,m^{-2}\,K^{-1}}$ (for water this is expressed in units of $\mathrm{J\,m^{-2}\,Pa^{-1}}$ and for CO_2 in units of $\mu\mathrm{mol\,m^{-2}\,Pa^{-1}}$). The introduction of the new prognostic variables, T_a, e_a and CO_{2_a} makes it possible to define the new fluxes, originating at the CAS level, which appear on the right hand side:

$$\begin{aligned} H_a &= \rho c_p \frac{(T_a - T_r)}{r_a} \\ E_a &= \frac{\rho c_p}{\gamma}\frac{(e_a - e_r)}{r_a} \\ F_{\mathrm{CO}_{2_a}} &= \kappa \frac{(\mathrm{CO}_{2_a} - \mathrm{CO}_{2_r})}{r_a} \end{aligned} \tag{6}$$

where γ is the psychrometric constant ($\mathrm{Pa\,K^{-1}}$) and κ a unit conversion ($\mu\mathrm{mol\,Pa^{-1}\,m^{-3}}$).

The prognostic equations in (5) smoothly reduce to the diagnostic expressions in (2) for the case of zero CAS thickness (e.g. for grasslands, although the canopy-reference level distance could also be much smaller in such a case), for example for the CAS temperature:

$$\lim_{c_a \to 0} c_a \frac{\partial T_a}{\partial t} = 0 \Rightarrow H_a = H_c + H_g \tag{7}$$

therefore, substituting from Eq. (6):

$$T_a = T_r + \frac{r_a(H_c + H_g)}{\rho c_p} \tag{8}$$

which is equivalent to the first diagnostic expressions in (2). The same applies to e_a and CO_{2_a}.

These new prognostic variables and definitions also greatly simplify the expressions for the partial derivative terms, eliminating the need to carry cross-derivative terms, for instance, in contrast to (4):

$$\frac{\partial H_c}{\partial T_c} = \frac{\rho c_p}{r_b} \tag{9}$$

because only the foliage and CAS temperatures are involved as independent variables. The same simplifications apply to all other cross-derivative terms and permits the overall elimination of 20 partial derivative terms which are programmed in different parts of the numerical implementation.

The new equation set that is formed by adding the three CAS prognostic equations to the set in (1) and by altering the definitions of the individual fluxes comprises the new SiB2 solution core, which will be called SiB2.5 thereafter. The discretization and solutions to the new core equation system are shown in Appendix A.

3. Off-line simulations with diagnostic and prognostic solutions

The two model versions, 2 (diagnostic CAS) and 2.5 (prognostic CAS) have been run off-line for six Fluxnet sites for years between 1996 and 1999. The individual simulations were driven by meteorological data, with an update frequency of 30 minutes and were spun up for 5 years prior to the actual integration. Initial and boundary conditions (especially time-dependent ones) were pre-calculated with a SiB2 accessory tool, Mapper, in the same way as described in Sellers et al. (1996a), using the EFAI data sets of Stöckli and Vidale (2004a). The reference level CO_{2_r} was fixed at 37.5 Pa, since it is not possible in off-line mode to simulate the boundary layer oscillation of CO_2 concentrations and it was deemed safer, at this stage, to keep this extra degree of freedom from influencing our assessment of the new model performance. The time step for the integrations is 10 minutes for both formulations. All integrations were continued for the period of availability of tower forcing data, which varies by site, but is always comprising of at least one full year of data. In this study we will provide examples from the Tharandt (Germany) site, while in the companion Stöckli and Vidale (2004b) we provide a much wider range of applications at different European sites. The Tharandt Fluxnet tower measures micrometeorological variables and radiation, heat, water and carbon fluxes in a coniferous forest (mean LAI of 6.0) and is located in Germany (50°58′N 13°38′E). The site has a mean annual temperature of 7.5 °C and receives 824 mm of rain (climatological yearly mean). We present observational data (publicly available through the Fluxnet database, http://www-eosdis.ornl.gov/FLUXNET/) and simulations for the year 1998. Data gap filling issues are discussed in Stöckli and Vidale (2004b).

4. Discussion

The novelty of this approach consists in the use of the storage capacities for the CAS variables, which allows for the 'memory' of the system, similar to what is done in the calculation of eddy correlation fluxes under a tower. This is particularly important at times of transition between a stable and an unstable surface layer, when differences arise in the two treatments, due to the existence of storage fluxes within the CAS.

The strong simplifications in the calculation of the cross-coupling terms has also allowed for a more streamlined discretization of the prognostic equations, for the numerical implementation, than in the previous framework. One of the practical consequences is the inclusion of fully implicit long wave radiative terms in the net radiation components, which within this framework requires minimal effort and is physically justified. As discussed in Bonan (1996), however, this extra increment term is usually smaller than the other forcings, although it can become comparatively important at particular times of the diurnal cycle. The details of this implementation are available in the appendix.

The analysis of the comparative performance of the two models focuses on the production of prognostic variables and on the fluxes originating in the CAS. Much more substantial validation and testing, focusing on heat and water fluxes over different Fluxnet sites has been performed in a companion paper, also in this issue (see Stöckli and Vidale, 2004b).

4.1 Simulation of the yearly and diurnal cycle of canopy temperatures

The canopy leaves temperature T_c is a primary prognostic variable in SiB2 and the evolution of an average diurnal cycle in July 1998 is shown in Fig. 2a for the Fluxnet site Tharandt; a complementary evolution is shown for the 1998 yearly temperature cycle in Fig. 2b. Comparisons with available observations shows that both model versions simulate the yearly cycle of temperature in a fairly accurate way, so that to the first order both solutions are compatible. This was also true of other sites and prognostic variables (not shown). The diurnal plots show that the July mean diurnal cycle is better simulated by SiB2.5, since SiB2 tends to be consistently too warm. For the yearly cycle, SiB2.0, however, provides a better simulation of winter time temperatures, but is too warm by about 2K over the summer. SiB2.5, on the other hand, tends to be cold in winter (2–3 K), but simulates the summer temperatures accurately. This is important for biophysical feedbacks in continental areas, involving physiological responses to too elevated maximum diurnal CAS temperatures during the late growing season, a problem common to many climate models (see e.g. the discussion in Vidale et al., 2003). An explanation for the winter-time temperature evolution in SiB2.5 is connected with both the extra stratification, provided by the new CAS layer, and with the more extreme r_a and r_d values, which can now be produced by the use of the prognostic T_a variable in the definition of the aerodynamic resistances. Other effects derive from storage fluxes, which are explored in the following subsection.

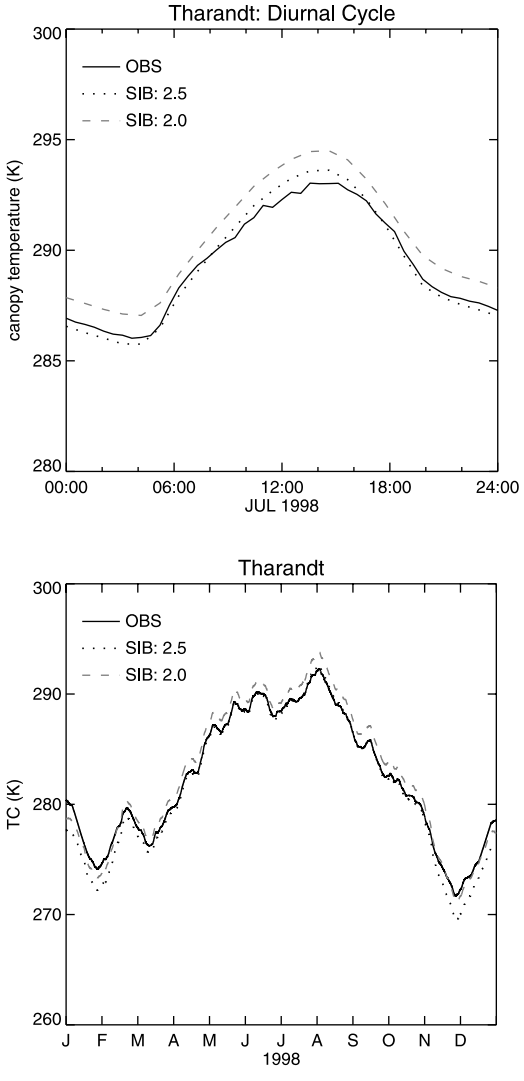

Fig. 2. Prognostic (SiB2 and SiB2.5) of canopy leaves temperature T_c (K) at Tharandt, 1998: **a**) average diurnal cycle (top) in July and **b**) yearly time series (bottom). Observations at the site are also shown for reference

4.2 Simulation of CAS storage fluxes

Canopy storage fluxes are only available at a few sites in the Fluxnet dataset; we use the data from Tharandt as an example. Figure 3 shows the latent and sensible heat storage fluxes at this site, as an average diurnal cycle for the entire year of 1998 (left panel). The data for July show that the SiB2.5 model is simulating the heat and water storage fluxes in the CAS in both magnitude (order of $10\,\mathrm{W\,m^{-2}}$) and phase. The right hand panel figures show the corresponding fluxes for the average diurnal cycle in the month of July 1998. The CAS is therefore a sink of heat in the early part of the day, and a source near sunset; for water, however, the CAS appears to function as a sink near both sunrise and sunset, in agreement with measured data. At these times CAS storage fluxes are at a maximum and time lags of up to 30 minutes appear in the surface soil/vegetation/atmosphere network; therefore storage fluxes will introduce a lag in the fluxes originating at the CAS. The same interpretation is valid for the seasonal cycle (not shown), in which periods of larger stability (and large values of aerodynamic resistances) will coincide with more storage and flux lag, while periods of lower

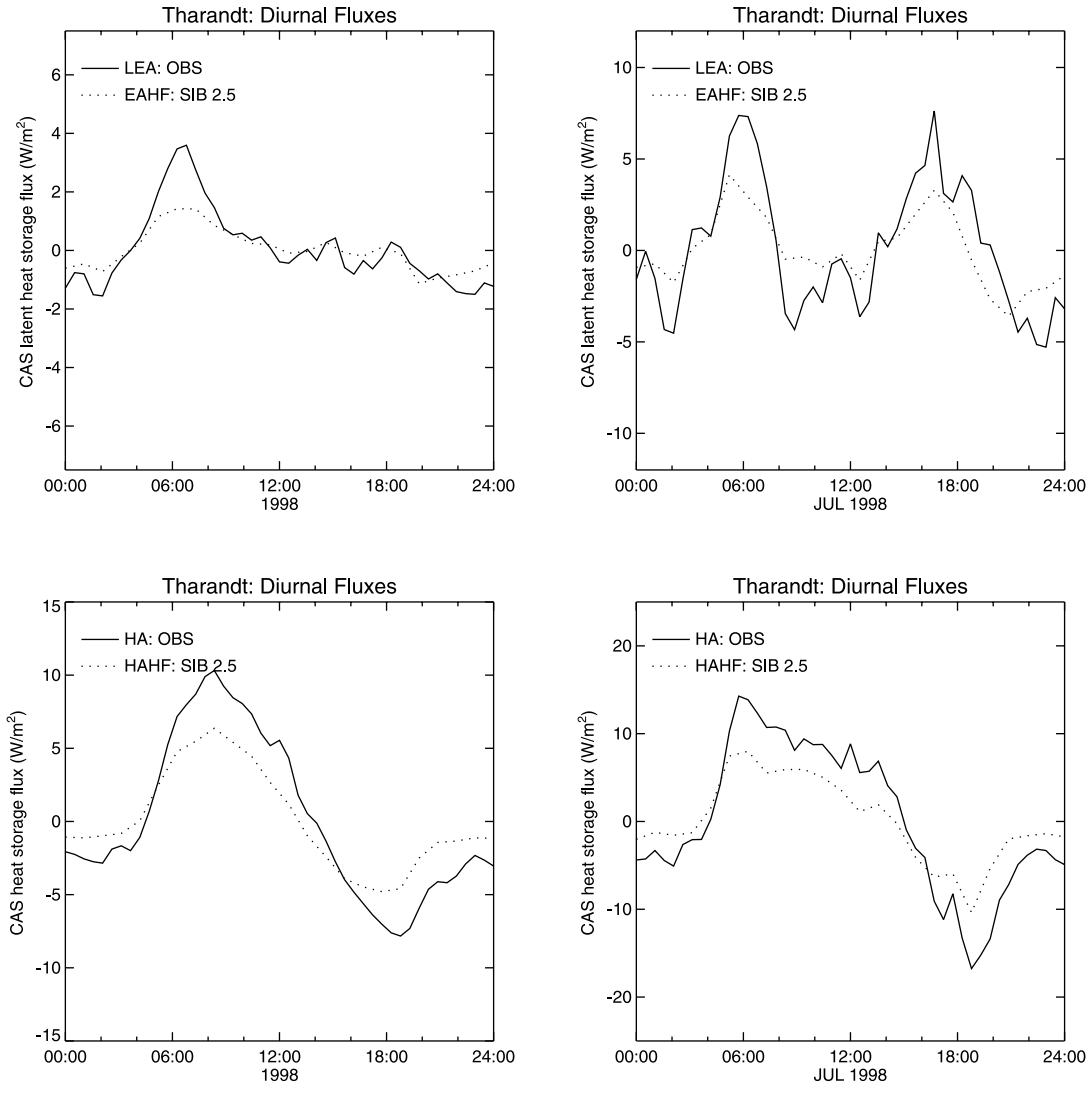

Fig. 3. The SiB2.5 CAS water (top) and heat (bottom) storage fluxes ($W\,m^{-2}$) for an average day in the year 1998 (left panels) and for an average day in July (right panels), Tharandt site. Measured values shown for reference

stability will see less storage, through diminished control imposed by the resistance network. The effects of these storage fluxes should become mostly evident in the CO_{2_a} evolution (see Fig. 4), which is controlled by two sources, one at the surface and one at the reference level, while being depleted by a single sink, at the canopy level.

4.3 Simulations of yearly and diurnal cycles of CO_2 partial pressures in the CAS

As explained in section 3, simulations were performed using a fixed reference level CO_2 partial pressure (37.5 Pa), which damps the diurnal cycle of CO_2, since no BL oscillation of CO_2 is fed to the model through the boundary data. The plots in Fig. 4 show the yearly cycle on the x axis and the diurnal cycle on the y axis. The middle figure shows the observed CO_2 at the reference level at Tharandt for 1998 for comparison, while the other two panels show the partial pressures predicted by SiB2 and SiB2.5. The CO_2 at the reference level is not expected to be depressed by assimilation as much as in the CAS during times of poor vertical mixing; it should not, however, display higher level of CO_2 than found in the CAS during periods of high stability. The model reproduces reasonably well the yearly and diurnal cycles of CO_2, which is high during the winter and night (high vertical stability and no assimilation) and low during the summer and

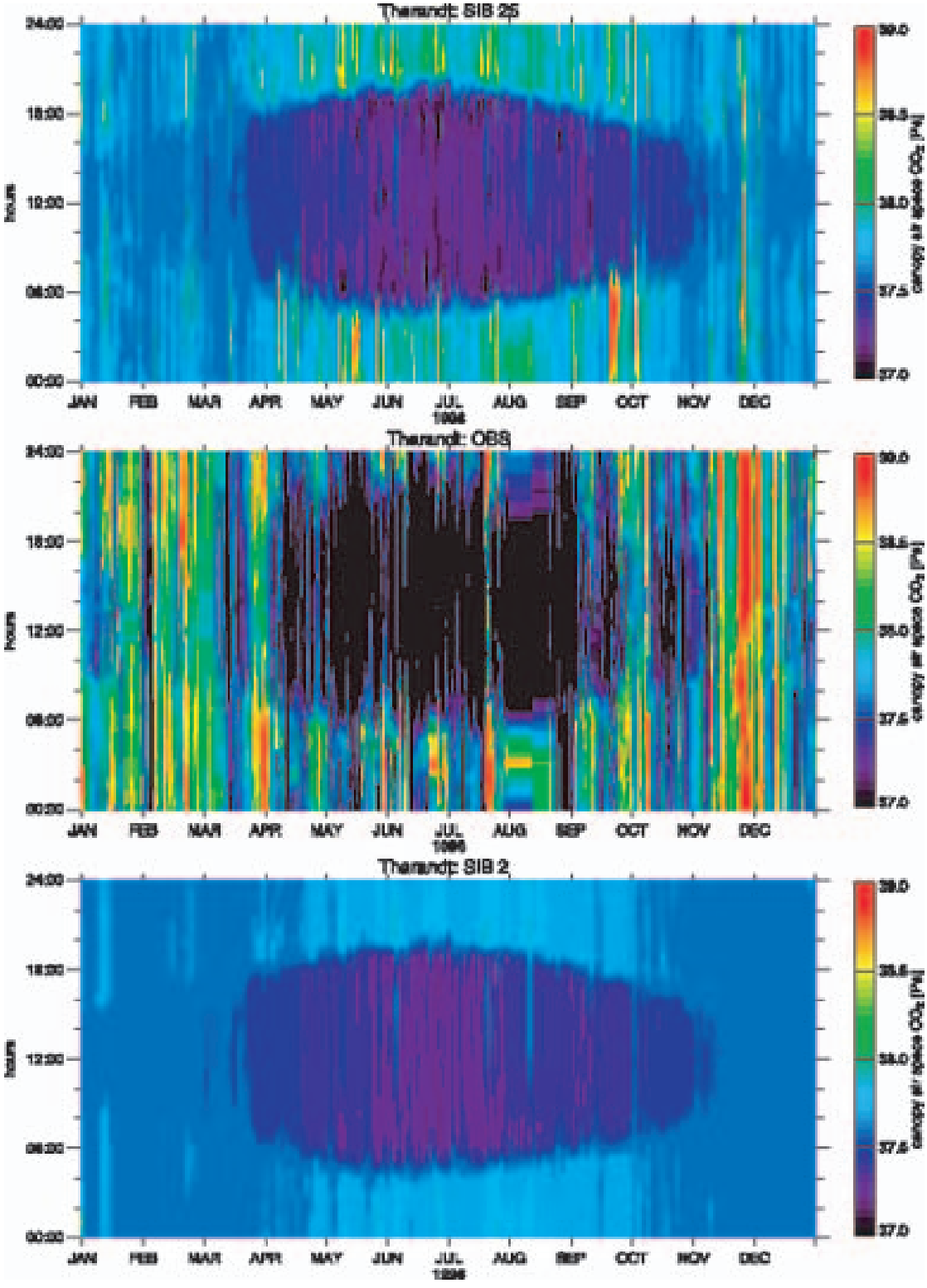

Fig. 4. Diurnal and yearly evolution of CAS level CO_2 partial pressure (Pa) at Tharandt, 1998 for the two model versions (SiB2.5 top and SiB2, bottom). The middle panel shows the reference level observed pressure for reference

at daytime (mixed SL and assimilation is active). The different solutions in SiB2 and SiB2.5 are most evident near times of stable stratification in the surface layer (that is, night time or winter), when storage and reduced transfer between the reference level and the land surface components

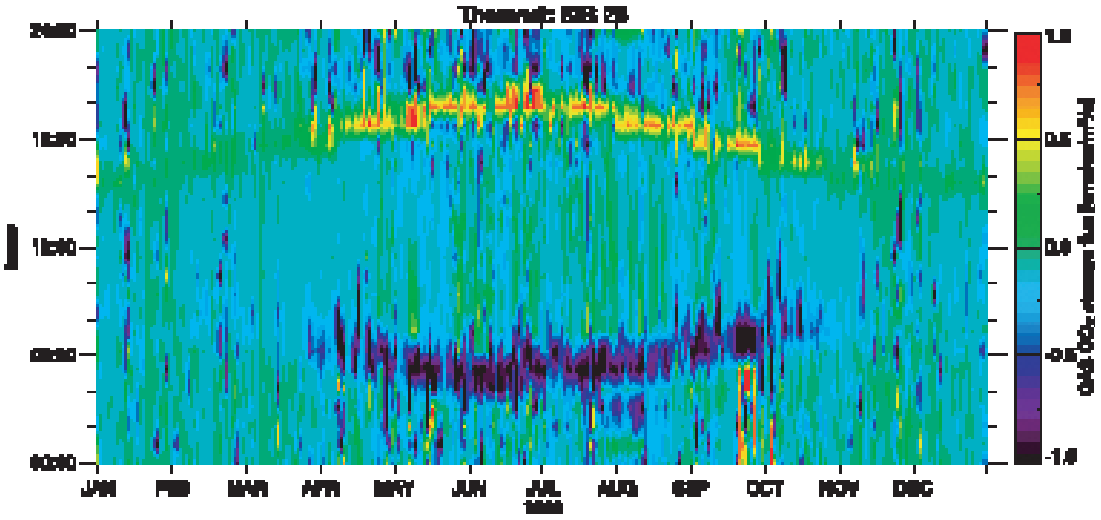

Fig. 5. The SiB2.5 CAS CO_2 storage fluxes ($\mu mol\, m^{-2}\, s^{-1}$) at Tharandt, 1998, diurnal and yearly cycles

allow the CAS to accumulate CO_2. In general SiB2.5 is able to represent the winter and nighttime accumulation of CO_2 near the surface much better than SiB2. The feedback effect deriving from the synergy of stability and source/sink activity has been denominated ''rectifier effect'' in Denning et al. (1996), but cannot be fully investigated here because of our off-line methodology. The characteristic of the new prognostic model, the lag introduced by the CAS capacities, seems to be consistent with the effect of storage fluxes.

4.4 Simulations of yearly and diurnal cycles of CO_2 storage fluxes in the CAS

An example of the yearly and diurnal cycles of CO_2 storage fluxes produced in SiB2.5 is given in Fig. 5, which shows how the CAS is acting as a CO_2 sink in the early hours of each day and as a source near sunset over an extended yearly cycle, from April until October. The magnitude of the fluxes, about 1 $\mu mol\, m^{-2}\, s^{-1}$, is about one order of magnitude less than the typical peak CO_2 flux (+5 at nighttime to $-20\, \mu mol\, m^{-2}\, s^{-1}$ during daytime), but quite relevant near the times of reversal of vertical stability, at sunset and sunrise. The ''signature'' of these fluxes appears therefore to be in agreement with theory and, by looking at the induced CO_2 partial pressures in the previous sections, also with observations.

4.5 Considerations on computing costs

The costs of a simulation with SiB2.5, for which three extra prognostic equations need to be solved, are offset by the overall reduction in accessory calculations (for the cross-derivative terms) and by faster convergence of the solutions. Overall, therefore, no significant changes in CPU requirements have been observed. The development and maintenance costs for the code have been greatly reduced through closer agreement of analytical and numerical solutions and through the elimination of a large number of cross derivative terms that need not be carried through the many different subroutines in the code.

5. Conclusions

A new solution core for the calculation of near-surface prognostics in an LSM has been developed and applied to the Sellers et al. (1996b) SiB2. The new approach consists of introducing canopy air space prognostic variables for CAS temperature (T_a), water (e_a) and carbon (CO_{2_a}), with corresponding storage capacities. The numerical implementation of the proposed prognostic approach introduced here has proven accurate, stable, efficient and above all easier to maintain than the diagnostic one it substitutes. We have applied the model to the off-line simulation of micrometeorological tower state variables, fluxes and concentrations from the Fluxnet project. Solutions for the prognostic variables show

that the quality of the forecasts is at least as good as the one of the diagnostic system, but further reassurance about the soundness of the solutions is provided by the derived storage fluxes signatures and by the comparison of accumulated CO_2 near the surface, especially at times of large vertical stability. The diurnal and yearly evolutions of CAS variables and fluxes show that the adoption of the CAS prognostics can therefore be justified for both physical and numerical reasons. The model has been more thoroughly tested and validated in terms of heat and water fluxes over a wider variety of sites and environmental conditions in a companion paper by Stöckli and Vidale (2004b). The next phase of the off-line simulations with similar micrometeorological data will include the introduction of time series of CO_2 concentrations at the reference level, in order to test the stability of the solutions and the magnitude of the response in a system with an extra degree of freedom. More dramatic effects are expected in coupled-mode experiments, in which the reference level CO_2 is allowed to oscillate freely; some of this work has already been accomplished in Denning et al. (2003) and Baker et al. (2003) for short-term studies.

Acknowledgments

This work was the result of cooperation with Prof. A. S. Denning and his group at Colorado State University, Fort Collins, CO, USA: P. L. Vidale initiated this work in 1998 while at CSU, and was supported at the time under grant US-DOE-NIGEC number DE-FC03-90ER61010. This research was later supported by the Swiss Ministry for Education and Science (BBW contract Nr. 97.008). The pre-processing of NDVI data used for driving SiB2 was accomplished at NASA Goddard, under contracts NAS5-01070, Task No. 4a, SSAI subcontract No. 2101-03-002. The original SiB2 model and all SiB2 pre-processing tools were also made available by Prof. Denning and his group. FLUXNET data were made available by R. Olson and E. Falge through the Fluxnet WWW site and CDROM.

Appendix A: Discretization and numerical solution of the land surface prognostic equations

The solution method, which lies at the heart of the Sato et al. (1989b) publication, simultaneously solves the system of equations for all state variables between the ground surface and the first atmospheric level (within the surface layer), including the canopy air space (CAS), having this general implicit-in-time form for each land surface prognostic variable in the LSM framework, S_x, similar to the treatment in Bhumralkar (1975):

$$c_x \frac{\partial S_x}{\partial t} = \sum F_x^{t+1}$$

which is discretized as:

$$c_x \frac{\Delta S_x}{\Delta t} \cong \sum \left(F_x^t + \frac{\partial F_x}{\partial t} \cdot \Delta t \right) \tag{A1}$$

where the t superscript is the time level and the x subscript refers to any component of the system, e.g. c for canopy leaves and a for CAS. The summation is over all relevant fluxes (F) for each variable. The original set of equations for the SiB2 LSM is described by Sato et al. (1989b) and by Sellers et al. (1996b) and comprises prognostic equations for T_g, T_c, and for soil water reservoirs.

The implementation corresponds to a backward implicit scheme in time. However, to be more general, when both left and right hand sides are at time level $t+1$, this is really an implicit system, if both are at time t, it is an open-explicit system, and, if any combination is applied, this corresponds to having a semi-implicit or even an explicit system, as discussed for instance in Polcher et al. (1998). In the original SiB2, parts of the right side were at time level t, so the system was semi-implicit. In the newer formulation presented here all terms but the resistance (r_x terms) network are at time $t+1$, making the new solution system, SiB2.5, fully implicit.

This set was solved with the "implicit with explicit coefficients" method of Sato et al. (1989b), which translates into using a truncated Taylor series approximation:

$$\begin{aligned} c_x \frac{\Delta S_x}{\Delta t} &\cong \sum \left(F_x^t + \frac{\partial F_x}{\partial S_x} \cdot \frac{\partial S_x}{\partial t} \cdot \Delta t \right) \\ &= \sum \left(F_x^t + \frac{\partial F_x}{\partial S_x} \cdot \Delta S_x \right) \end{aligned} \tag{A2}$$

which forms the basis of the numerical model implementation, solving for the finite differences ΔS_x as in Sato et al. (1989b), Sellers et al. (1996b) and Randall et al. (1996).

Thus, starting with the Sellers et al. (1996b) Eq. (1) through (3), and following the solution procedure implemented by Sato et al. (1989b) in Eq. (1) through (5), the new (5×5) system of equations is:

$$\begin{aligned} &\left(\frac{c_c}{\Delta t} + \frac{\partial H_c}{\partial T_c} + \frac{\partial E_c}{\partial T_c} + \frac{\partial L_c}{\partial T_c} \right) \Delta T_c + \frac{\partial L_c}{\partial T_g} (1 - A_s) \Delta T_g \\ &\quad + \frac{\partial L_c}{\partial T_s} (A_s) \Delta T_s + \frac{\partial H_c}{\partial T_a} \Delta T_a + \frac{\rho c_p}{\gamma} \frac{\partial e_c}{\partial e_a} \Delta e_a \\ &\quad = R_{net_c}^t - H_c^t - E_c^t \end{aligned} \tag{A3}$$

$$\begin{aligned} &\frac{\partial L_g}{\partial T_c} \Delta T_c + \left(\frac{c_g}{\Delta t} + \frac{\partial H_g}{\partial T_g} + \frac{\partial E_g}{\partial T_g} + \frac{\partial L_g}{\partial T_g} + S_\lambda \right) \Delta T_g \\ &\quad + \frac{\partial H_g}{\partial T_a} \Delta T_a + \frac{\rho c_p}{\gamma} \frac{\partial e_g}{\partial e_a} \Delta e_a = R_{net_g}^t - H_g^t \\ &\quad - E_g^t - S_\lambda (T_g^t - T_d^t) \end{aligned} \tag{A4}$$

$$\begin{aligned} &\frac{\partial L_s}{\partial T_c} \Delta T_c + \left(\frac{c_s}{\Delta t} + \frac{\partial H_s}{\partial T_s} + \frac{\partial E_s}{\partial T_s} + \frac{\partial L_s}{\partial T_s} + S_\lambda \right) \Delta T_s \\ &\quad + \frac{\partial H_s}{\partial T_a} \Delta T_a + \frac{\rho c_p}{\gamma} \frac{\partial e_s}{\partial e_a} \Delta e_a = R_{net_s}^t - H_s^t \\ &\quad - E_s^t - S_\lambda (T_s^t - T_d^t) \end{aligned} \tag{A5}$$

$$-\frac{\partial H_c}{\partial T_c}\Delta T_c-\frac{\partial H_g}{\partial T_g}(1-A_s)\Delta T_g-\frac{\partial H_s}{\partial T_s}A_s\Delta T_s+\frac{\partial H_a}{\partial T_r}\Delta T_r+\left(\frac{c_a}{\Delta t}-\frac{\partial H_c}{\partial T_a}+\frac{\partial H_a}{\partial T_a}-(1-A_s)\frac{\partial H_g}{\partial T_a}-A_s\frac{\partial H_s}{\partial T_a}\right)\Delta T_a=H_c^t-H_a^t+(1-A_s)H_g^t+A_sH_s^t \quad \text{(A6)}$$

$$-\frac{\partial E_c}{\partial T_c}\Delta T_c-\frac{\partial E_g}{\partial T_g}(1-A_s)\Delta T_g-\frac{\partial E_s}{\partial T_s}A_s\Delta T_s+\frac{\partial E_a}{\partial e_r}\Delta e_r+\left(\frac{c_a}{\Delta t}-\frac{\partial E_c}{\partial e_a}+\frac{\partial E_a}{\partial e_a}-(1-A_s)\frac{\partial E_g}{\partial e_a}-A_s\frac{\partial E_s}{\partial e_a}\right)\Delta e_a=E_c^t-E_a^t+(1-A_s)E_g^t+A_sE_s^t \quad \text{(A7)}$$

where the usual variable indexes apply, with the introduction of T_s, A_s for snow temperature (K) and area extent (%), and L_x for emitted longwave fluxes from each component ($\mathrm{W\,m^{-2}}$), so that, for instance, ΔT_c is the leaves temperature increment (K); ΔT_a is the CAS temperature increment (K); ΔT_g is the bare ground surface temperature increment (K); ΔT_s is the snow temperature increment (K); ΔT_r is the reference level temperature increment (K); Δe_a is the CAS vapor pressure increment (Pa); Δe_r is the reference level vapor pressure increment (Pa); c_c is the leaves heat capacity ($\mathrm{J\,m^{-2}\,K^{-1}}$); c_a is the CAS heat capacity ($\mathrm{J\,m^{-2}\,K^{-1}}$); c_g is the bare ground heat capacity ($\mathrm{J\,m^{-2}\,K^{-1}}$); c_s is the snow heat capacity ($\mathrm{J\,m^{-2}\,K^{-1}}$); H is the sensible heat flux ($\mathrm{W\,m^{-2}}$); E is the latent heat flux ($\mathrm{W\,m^{-2}}$); S_λ is the exchange coefficient for the ground heat flux ($\mathrm{J\,m^{-2}\,K^{-1}\,s^{-1}}$). For the water variables, the capacities are in $\mathrm{J\,m^{-2}\,Pa^{-1}}$.

The temperatures of ground and snow at time t (right hand side of equations) are the same, prior to each time step, since energy exchanges and areal adjustments involving snow growth/melting are carried out between time steps. Only the time increments ΔT_g and ΔT_s are allowed to diverge into separate solutions during the simultaneous solution calculation; by the time the next prognostic time step is reached the two temperatures will be once more identical.

This system of equations is solved simultaneously by Gaussian elimination at each time step. Within the CSU GCM Randall et al. (1996), it is also possible to solve simultaneously for the evolution of the bulk mixed layer prognostic (reference) variables as influenced by surface fluxes. This option is inactive when the model is run off-line (thus the reference level variables represent boundary conditions) or when the model is coupled to a host atmospheric model that has a discrete multi-layer treatment of the boundary layer. This raises the number of equations to be simultaneously solved to 7×7.

$$-\frac{\partial H_a}{\partial T_a}\Delta T_a+\left(\frac{c_r}{\Delta t}+\frac{\partial H_a}{\partial T_r}\right)\Delta T_r=H_a^t \quad \text{(A8)}$$

$$-\frac{\partial E_a}{\partial T_a}\Delta T_a+\left(\frac{c_r}{\Delta t}+\frac{\partial E_a}{\partial e_r}\right)\Delta e_r=E_a^t \quad \text{(A9)}$$

where ΔT_r is the reference level temperature increment (K); Δe_r is the reference level vapor pressure increment (Pa); c_r is the reference level heat capacity ($\mathrm{J\,m^{-2}\,K^{-1}}$or $\mathrm{J\,m^{-2}\,Pa^{-1}}$ for vapor pressure).

The expression for the individual (H and E) fluxes remains identical to the ones in Table 4, Sellers et al. (1996b), while it is their derivatives that are now simplified. The only new expressions are the ones relative to the total surface fluxes of heat and water, which are:

$$H_a=\rho c_p\frac{T_a-T_r}{r_a};\qquad E_a=\frac{\rho c_p}{\gamma}\frac{e_a-e_r}{r_a} \quad \text{(A10)}$$

The expressions for the individual resistances, r_b, r_d, r_a, r_c are now true to their definition, once T_a is now a prognostic variable and thus can be included in those equations (see the discussion on page 685 of Sellers et al., 1996b).

In SiB2 stomatal conductance is calculated through the Ball-Berry equation, Ball et al. (1987), Ball (1988), which relates carbon assimilation to the loss of water through the stomata. This computation is necessary to determine transpiration rates, but also concludes the updating of the resistance network prior to the simultaneous calculation of the surface prognostic variables and will also determine the carbon flux from the surface to the first atmospheric level, according to Eq. (6).

Appendix B: Energy and water limitations in the implicit solution system

The partial derivative terms appearing in Eqs. (A3–7) can potentially violate water conservation, since they implicitly depend on temperature increments in the prognostic time step, which makes it difficult to establish, a priori, that water reservoirs in the canopy, soil and at the ground surface will not be exhausted during the time step.

In SiB2 a complex system of energy and water checks was responsible for restoring water levels to conservative amounts after a time step in which they had been exhausted, converting the excess latent heat into sensible heat.

In the new solution core, this system is both undesirable and unnecessary and the following criteria are used in order to guarantee that the "flux payback" system is not activated.

$$\begin{aligned}\frac{\partial E_{ci}}{\partial t}\Delta t&\cong\frac{\partial E_{ci}}{\partial T}\Delta T_c\le\alpha\lambda W_{ci}\\ \frac{\partial E_{ct}}{\partial t}\Delta t&\cong\frac{\partial E_{ct}}{\partial T}\Delta T_c\le\alpha\lambda W_{gd}\\ \frac{\partial E_{gs}}{\partial t}\Delta t&\cong\frac{\partial E_{gs}}{\partial T}\Delta T_g\le\alpha\lambda W_{gs}\\ \frac{\partial E_{gi}}{\partial t}\Delta t&\cong\frac{\partial E_{gi}}{\partial T}\Delta T_g\le\alpha\lambda W_{gi}\end{aligned} \quad \text{(B1)}$$

where W_x are the water reservoirs (kg). Subscripts i and t refer, respectively, to interception and transpiration, while d and s refer to deep (root zone) and superficial (upper soil level). The security constant α is specified (currently 0.75) and meant to prevent the exhaustion of any reservoir over a single time step. For this specific set of secondary calculations (which are found to have a contribution much smaller than the balance of fluxes to the right of A3–7), a maximum possible ΔT of 3 K and Δe of 500 Pa for each individual component over each time step is also imposed in order to solve the system, with the result of "slowing down" the time evolution of each prognostic as forced by these secondary feedback mechanisms.

Evaporation from individual reservoirs is also limited by energy availability:

$$\frac{\partial E_{ci}}{\partial t}\Delta t \cong \frac{\partial E_{ci}}{\partial T}\Delta T_c \leq \beta R_{n_c}$$
$$\frac{\partial E_{ct}}{\partial t}\Delta t \cong \frac{\partial E_{ct}}{\partial T}\Delta T_c \leq \beta R_{n_c}$$
$$\frac{\partial E_{gs}}{\partial t}\Delta t \cong \frac{\partial E_{gs}}{\partial T}\Delta T_g \leq \beta R_{n_g}$$
$$\frac{\partial E_{gi}}{\partial t}\Delta t \cong \frac{\partial E_{gi}}{\partial T}\Delta T_g \leq \beta R_{n_g} \quad \text{(B2)}$$

where β is a security constant (currently 0.5) meant to energetically limit the exhaustion of each reservoir over a single time step.

From these expressions it is possible to derive the limitations to the partial derivatives of vapor pressure with relation to temperature that are to be used in the solution core (previous section) so that no reservoir will be exhausted a priori during a single time step. A maximum possible ΔT of 3 K for each component over one time step is also imposed here.

These criteria have been discussed for completeness, despite their triggering conditions being hardly ever activated in the operation of the SiB2.5 version which we have presented. The inclusion of such safety criteria has become completely unnecessary after the implementation of a new multi-layer soil moisture scheme, a recent development not addressed in this manuscript.

References

Arora VK (2002) Modeling vegetation as a dynamic component in soil-vegetation–atmosphere transfer schemes and hydrological models. Rev Geophys 40(2): 3-1–3-27

Baker I, Denning AS, Hanan N, Prihodko L, Uliasz M, Vidale PL, Davis K, Bakwin P (2003) Simulated and observed fluxes of sensible and latent heat and CO_2 at the WLEF-TV tower using SiB2.5. Glob Change Biol 9: 1262–1277

Baldocchi D, Falge E, Gu L, Olson R, Hollinger D, Running S, Anthoni P, Bernhofer Ch, Davis K, Evans R, Fuentes J, Goldstein A, Katul G, Law B, Lee X, Malhi Y, Meyers T, Munger W, Oechel W, Paw U KT, Pilegaard K, Schmid HP, Valentini R, Verma S, Vesala T, Wilson K, Wofsyn S (2001) Fluxnet: a new tool to study the temporal and spatial variability of ecosystem-scale carbon dioxide, water vapor, and energy flux densities. Bull Amer Meteor Soc 82(11): 2415–2433

Ball JT, Woodrow IE, Berry JA (1987) A model predicting stomatal conductance and its contribution to the control of photosynthesis under different environmental conditions, vol 4. In: Biggins J (ed) Progress in photosynthesis research. Dordrecht: M. Nijhoff Publishers, pp 221–224

Ball JT (1988) An analysis of stomatal conductance. PhD thesis, Department of Biological Sciences, Stanford University, 89 pp

Bhumralkar CM (1975) Numerical experiments on the computation of ground surface temperature in atmospheric general circulation models. J Appl Meteorol 14: 1246–1258

Bonan GB (1996) A land surface model (lsm version 1.0) for ecological, hydrological, and atmospheric studies: technical description and user's guide. NCAR Technical Note NCAR/TN-417 + STR, NCAR, Boulder, Colorado USA

Denning AS, Nicholls M, Prihodko L, Baker I, Vidale PL, Davis K, Bakwin P (2003) Simulated variations in atmospheric CO_2 over a Wisconsin forest using a coupled ecosystem–atmosphere model. Glob Change Biol 9: 1241–1250

Denning AS, Randall DA, Collatz GJ, Sellers PJ (1996) Simulations of terrestrial carbon metabolism and atmospheric CO_2 in a general circulation model. Part 2: spatial and temporal variations of atmospheric CO_2. Tellus 48B: 543–567

Dickinson RE, Henderson-Sellers A, Kennedy PJ (1993) Biosphere–atmosphere transfer scheme (bats) version 1e as coupled to the ncar community climate model. NCAR Technical Note NCAR/TN-387 + STR, NCAR

Kim W, Arai T, Kanae S, Oki T, Musiake K (2001) Application of the simple biosphere model (SiB2) to paddy field for a period of growing season in game-tropics. J Met Soc Japan 79: 387–400

Pielke RA (2001) Present and future of modeling global environmental change: toward integrated modeling, chapter Earth System Modeling–An Integrated Assessment Tool for Environmental Studies, pp 311–337. TERRAPUB

Polcher J, McAvaney B, Viterbo P, Gaertner M-A, Hahmann A, Mahfouf J-F, Noilhan J, Phillips T, Pitman A, Schlosser CA, Schulz J-P, Timbal B, Verseghy D, Xue Y (1998) A proposal for a general interface between land surface schemes and general circulation models. Global Planet Change 19: 261–276

Randall DA, Dazlich DA, Zhang C, Denning AS, Sellers PJ, Tucker CJ, Bounoua L, Los SO, Justice CO, Fung I (1996) A revised land surface parameterization (SiB2) for GCMs .3. The greening of the Colorado State University general circulation model. J Climate 9: 738–763

Sato N, Sellers PJ, Randall DA, Schneider EK, Shukla J, Kinter J, Hou Y-T, Albertazzi ER (1989a) Effects of implementing the simple biosphere model (SiB) in a gcm. J Atmos Sci 46: 2757–2782

Sato N, Sellers PJ, Randall DA, Schneider EK, Shukla J, Kinter J, Hou Y-T, Albertazzi ER (1989b) Effects of implementing the simple biosphere model (SiB) in a gcm: methodology and results. Technical report [Available from NASA HQ, Independence Avenue, Washington, D.C. 20545, USA]

Schmid HP, Su HB, Vogel CS, Curtis PS (2003) Ecosystem–atmosphere exchange of carbon dioxide over a mixed hardwood forest in northern lower michigan. J Geophys Res-Atmos 108: 4417

Sellers PJ, Dickinson RE, Randall DA, Betts AK, Hall FG, Berry JA, Collatz GJ, Denning AS, Mooney HA, Nobre CA, Sato N, Field CB, Henderson-Sellers A (1997) Modeling the exchanges of energy, water, and carbon between continents and the atmosphere. Science 275(5299): 502–509

Sellers PJ, Los SO, Tucker CJ, Justice CO, Dazlich DA, Collatz GJ, Randall DA (1996a) A revised land surface

parameterization (SiB2) for atmospheric GCMs. 2. The generation of global fields of terrestrial biophysical parameters from satellite data. J Climate 9: 706–737

Sellers PJ, Randall DA, Collatz GJ, Berry JA, Field CB, Dazlich DA, Zhang C, Collelo GD, Bounoua L (1996b) A revised land surface parameterization (SiB2) for atmospheric GCMs .1. Model formulation. J Climate 9: 676–705

Stöckli R, Vidale PL (2004a) European plant phenology and climate as seen in a 20-year AVHRR land-surface parameter dataset. Int J Remote Sensing 25(17): 3303–3330

Stöckli R, Vidale PL (2004b) Modeling seasonal water and heat exchanges at European uxnet sites. Theor Appl Climatol (this issue)

Vidale PL, Luthi D, Frei C, Seneviratne SI, Schar C (2003) Predictability and uncertainty in a regional climate model. J Geophys Res-Atmos 108: 4586

Walko RL, Band LE, Baron J, Kittel TGF, Lammers R, Lee TJ, Ojima D, Pielke RA Sr, Taylor C, Tremback CJ, Vidale PL, Tague C (2000) Coupled atmosphere–biophysics–hydrology models for environmental modeling. J Appl Meteorol 39: 931–944

Authors' address: P. L. Vidale (e-mail: pier-luigi.vidale@env.ethz.ch) and R. Stöckli (e-mail: stockli@env.ethz.ch), Institute for Atmospheric and Climate Science, ETH, Winterthurerstrasse 190, 8057 Zürich, Switzerland.